JOINT INVERSION FOR 3-DIMENSIONAL S-VELOCITY MANTLE STRUCTURE ALONG THE TETHYAN MARGIN

Suzan van der Lee[1], Sung-Joon Chang[1], Megan P. Flanagan[2], Heather Bedle[1], Federica Marone[3], Eric M. Matzel[2], Michael E. Pasyanos[2], Arthur Rodgers[2], Barbara Romanowicz[3], and Christian Schmid[4]

Northwestern University[1], Lawrence Livermore National Laboratory[2], UC Berkeley[3], and ETH Zurich[4]

ABSTRACT

For purposes of studying the lateral heterogeneity as well as for ultimately predicting seismograms for this region, we construct a new 3-D S-velocity model by jointly inverting a variety of different seismic data. We jointly invert regional waveforms, surface wave group velocity measurements, teleseismic *S* arrival times, and crustal thickness estimates from receiver functions, refraction lines, and gravity surveys. These data types have complementary resolving power for crust and mantle structures, vertical and lateral variations, shallow and deep mantle features, local and global structure. Therefore, a joint inversion of these data sets might help unravel the complexity of this tectonically diverse area. These measurements are made from a combination of mantle investigation of the deep suture between Europe and Africa (MIDSEA), Program for Array Seismic Studies of the Continental Lithosphere (PASSCAL), GeoScope, Geofon, Global Seismographic Network (GSN), International Deployment of Accelerometeres (IDA), MedNet, national networks, and local deployments throughout the study region which extends from the western Mediterranean region to the Hindu Kush and encompasses northeastern Africa, the Arabian peninsula, the Middle East, and part of the Atlantic Ocean for reference. We have fitted the waveforms of regional S and Rayleigh waves from over 3800 seismograms using Partitioned Waveform Inversion. We include over 3000 crustal thickness estimates from receiver functions, gravity measurements, and refraction profiles. We include Rayleigh wave group velocities for hundred thousands of paths transecting the region. We have over 3000 teleseismic S arrival times measured through cross correlation and over 170000 from picks originally reported to the International Seismological Centre (ISC). We demonstrate our inversion methodology and discuss results from combining these new measurements in a joint inversion for a three-dimensional S-velocity model. Finally, we will compute synthetic seismograms and travel-time surfaces through the new model.

OBJECTIVES

Our primary objective is developing a new 3-D *S*-velocity model for the Middle East and Mediterranean region, including North Africa, southern Europe, and Arabia that

1) is resolved in aseismic regions,
2) is resolved throughout the upper mantle (to 660 km),
3) resolves laterally varying crustal thickness,
4) contains laterally varying vertical velocity gradients,
5) is simultaneously compatible with multiple data sets,
6) utilizes several recent, unique waveform data sets, and
7) includes uncertainties of the model parameters.

These features would increase the model's ability to predict and calibrate regional travel times and waveforms, thereby providing improved event locations, focal mechanisms, and other event discriminants.

Secondly, we aim to convert the 3-D *S*-velocity model to a 3-D *P*-velocity model, using both literature on elastic properties (and their partial derivatives with temperature and pressure) of mantle rocks and empirical information provided by measured arrival times of teleseismic *P* and *Pms* waves.

Our third objective is to test both the *S*-and *P*-wave models' ability to predict regional *P* and *S* travel times, deflect wave paths and deform waveforms, and assess their effects first on the studied seismograms (travel times and amplitudes) and subsequently on the 3-D models derived from these data.

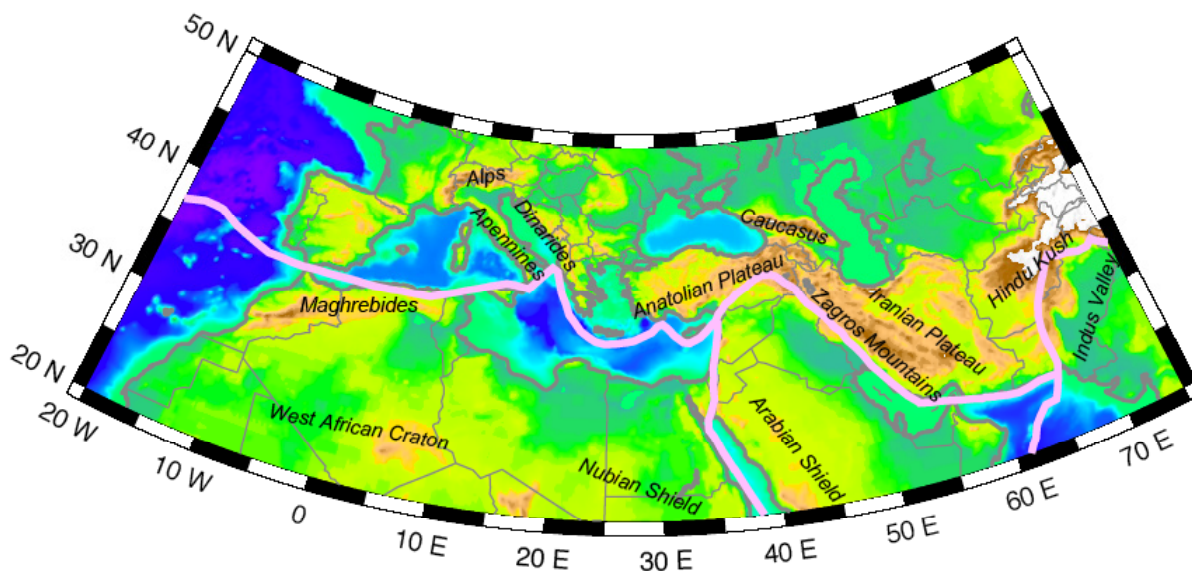This report focuses on the primary objective, a new 3-D *S* velocity model.

Figure 1. Topographic map of the study region. The pink line is the NUVEL1-A (DeMets et al., 1990) representation of the Eurasia-Africa-Arabia plate boundary. The study region is one of most tectonically complex in the world and is characterized by strong lateral variations.

The study region is centered around the Africa-Arabia-Eurasia triple junction (Figure 1), and extends west to the Africa-Eurasia-North America junction at the Azores, just off the map, and east to the Arabia-Eurasia-Indian Plate junction. The NUVEL1-A (DeMets et al., 1990) representation of these plate boundaries is shown by the pink line in Figure 1. The interaction of these six major tectonic plates with each other and with several microplates within an area of one quarter of the Earth's circumference yields this region rich with tectonic complexity. The three-dimensional structure of the upper mantle and crust are correspondingly complex. For example, while our region comprises only a few percent of the Earth's surface, it is home to more than half of all crustal types defined by

Mooney et al. (1998) to describe the Earth's crust globally. At the same time, the region is home to one of the most pervasive, though laterally varying low-velocity layers found beneath continental regions, which is interspersed with high-velocity bodies, related to Tethyan subduction, that extend hundreds of km vertically through the upper mantle and into the lower mantle (Van der Lee, 1990; Bijwaard et al., 1998; Marone et al., 2004; Schmid et al., 2007). We plan to capture various renditions of this structurally complicated part of the world in one *S*-velocity model through the joint inversion of several different types of seismic data simultaneously; the new model will refine our understanding of the structure and tectonics in this region of the Earth. The data types we combine are constraints from independent studies on the depth to the Moho, fundamental-mode Rayleigh-wave group velocity measurements, waveform fits of regional S and Rayleigh waves, and arrival times of teleseismic *S* waves.

RESEARCH ACCOMPLISHED

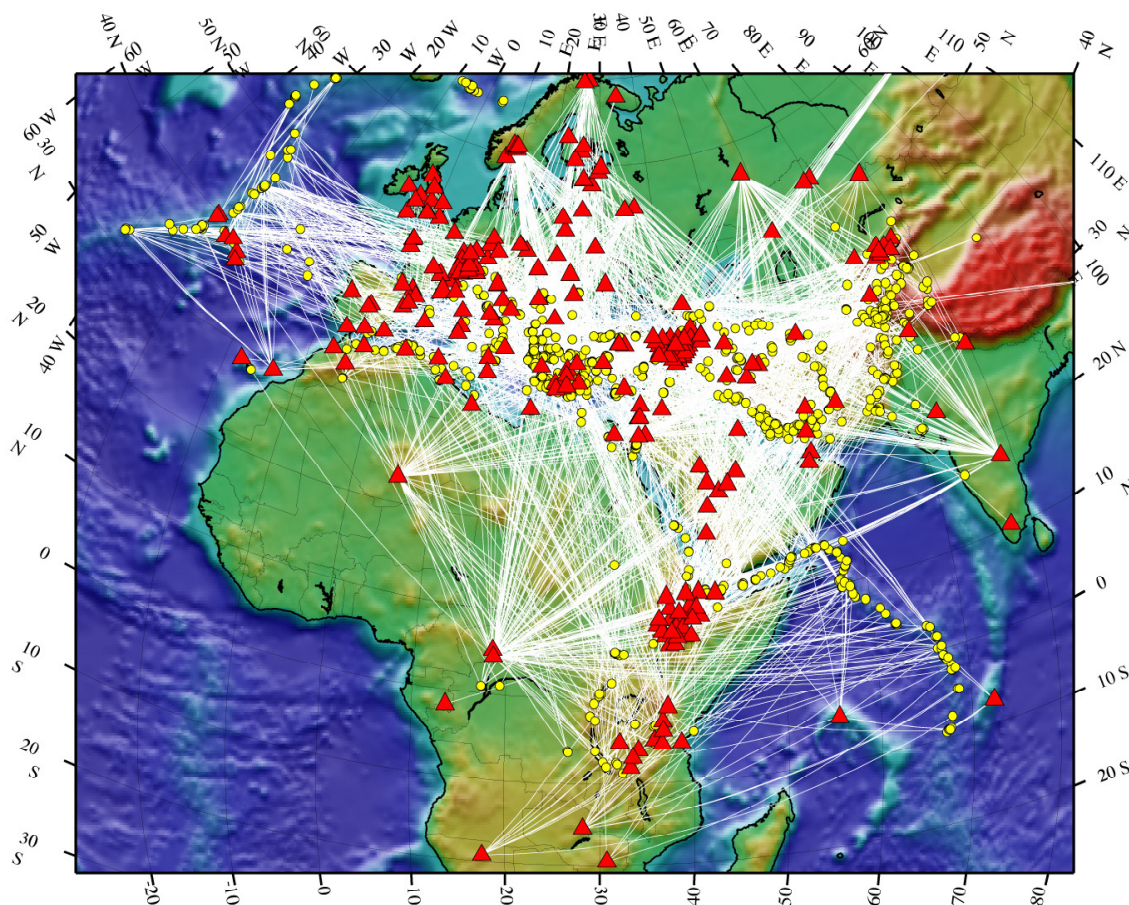**Figure 2. Map of raypath coverage showing all source-receiver paths for the region combining events (yellow circles) with Mb > 5.0 to all recording broadband stations (red triangles) at offsets between 5 and 50 degrees. This represents approximately 3,800 paths from both MIDSEA and LLNL databases.**

Regional Waveform Fits

We have examined over 13,000 available waveforms from the Lawrence Livermore National Laboratory (LLNL) database which sample North Africa and the Middle East and successfully fit about 3800 of them using the non-linear inversion procedure employed by previous partitioned waveform inversion studies (Van der Lee and Nolet, 1997; Marone et al., 2004). The great-circle wave paths for these seismograms are shown in Figure 2. We have estimated path-averaged S-velocity structures for these paths using the same starting S-velocity model but a different crustal thickness (in 5 km increments) for each path, based on a priori reported estimates (Van der Lee and Nolet,

1997; Marone et al., 2004). The starting model often predicts significant phase differences relative to the data for both the S- and Rayleigh waves. The inversion procedure estimates the perturbations to the starting model by non-linear optimization (Nolet, 1990; van der Lee and Nolet, 1997). For the computation of synthetic waveforms we also need to know the source mechanisms of the events. We typically use the centroid moment tensors (CMT) from the Harvard or Global CMT project, and hypocenters from Engdahl's reprocessed ISC database. The frequency content of the data and synthetic is different for each fit and generally falls within the band 0.006 to 0.1 Hz.

The optimal shear-velocity models for some of the paths in Figure 2 have shown: 1) faster crustal velocities and slightly faster mantle velocities for the Nubian shield, which is consistent with work by Mokhtar and Al-Saeed (1994), Sandvol et al. (1998), Rodgers et al. (1999), and Julia et al. (2003); 2) lower velocities in the crust and upper mantle for path crossing the East African Rift; 3) faster crustal and low sub-Moho velocities path from the Gulf of Aden across the Arabian Shield; and 4) faster velocities for paths traversing the Russian Platform to the north. It is worth noting that the Red Sea broke up the Nubian-Arabian Shield and these provinces could have similar crustal petrology. Both provinces have volcanics and it has been speculated that mafic intrusion may explain the higher crustal velocities. The inferred mantle velocities beneath the Nubian Shield are slightly faster than the starting model. However, reported mantle velocities beneath the Arabian Shield are lower than average (e.g., Mokhtar and Al-Saeed, 1994; Rodgers et al., 1999, Maggi and Priestley, 2005).

 The total ray path coverage is extensive from both the original MIDSEA dataset (Marone et al., 2004) and from data in the LLNL database (shown in Figure 2). We are able to extend the model area significantly to the east and achieve dense sampling of the Arabian Shield, Iran, Afghanistan, and Pakistan. We also have good coverage of northeast Africa, the Red Sea, and parts of the Russian Platform. We combine the 1-D, path-averaged, constraints obtained from these ~3,800 waveform fits with other data sets in the joint inversion for shear velocity structure.
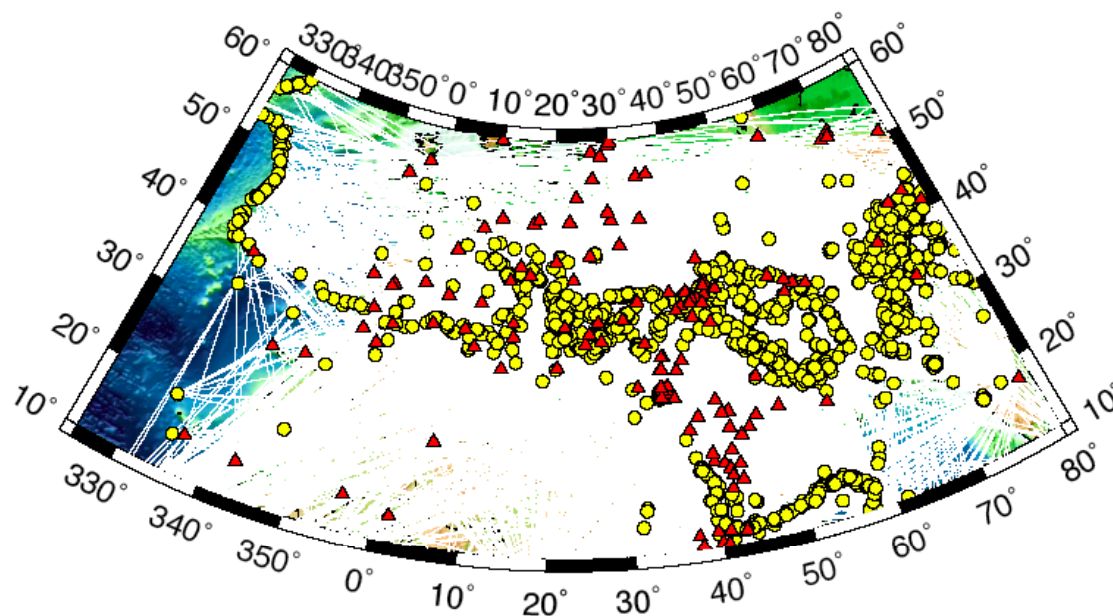
Surface Wave Group Velocities

Figure 3. Total wave path coverage for the Rayleigh-wave group velocity data set. Yellow dots are earthquakes, and red triangles are seismic stations. White lines are great-circle wave paths.

We have measured group velocities of fundamental-mode Rayleigh waves recorded at MIDSEA and other stations in the region and used them to update previous group velocity maps (e.g., Pasyanos, 2005). Figure 3 shows the

great-circle wave paths for which we included fundamental-mode Rayleigh wave group velocities in our joint inversion. Compared to other data types we include, lateral coverage is best for this group velocity data set, though vertical coverage is provided mainly by the teleseismic arrival times (Figure 5) and regional *S* and Rayleigh waveforms (Figure 2).

Pasyanos (2005), for example, used these group velocities in a typical two-step inversion process, first inverting for lateral variations in group velocity for a given frequency of the Raleigh wave and then inverting the group velocities for different frequencies at a given locality for a local shear-velocity model. To allow a self-consistent treatment of all data in our joint inversion we modified these steps such that first we express the measured group velocities as path-averages and integrals over the *S*-velocity distribution with depth. For each path we thus obtain as many constraints on the laterally averaged *S*-velocity as we have measurements at different periods. Typically these equations have a high degree of redundancy with respect to describing the S-velocity distribution with depth and are far from independent. We distill the most powerful constraints out of each such set of equations using a singular value decomposition to recombine the equations into independent ones and discarding constraints associated with small singular values. This process also provides meaningful error estimates that we later use to weight the constraints with smaller error estimates more strongly during the joint inversion. We then solve these subsets of equations for the 3-D S-velocity distribution by combining all of them, with or without constraints from our other data sets, in a single, linear, least-squares, joint inversion. We benchmarked this new 2-step procedure against S-velocity models obtained with the traditional 2-step procedure and find that it performs well and efficiently. The added advantage is that we can jointly and self-consistently invert the group velocity data together with our other data.
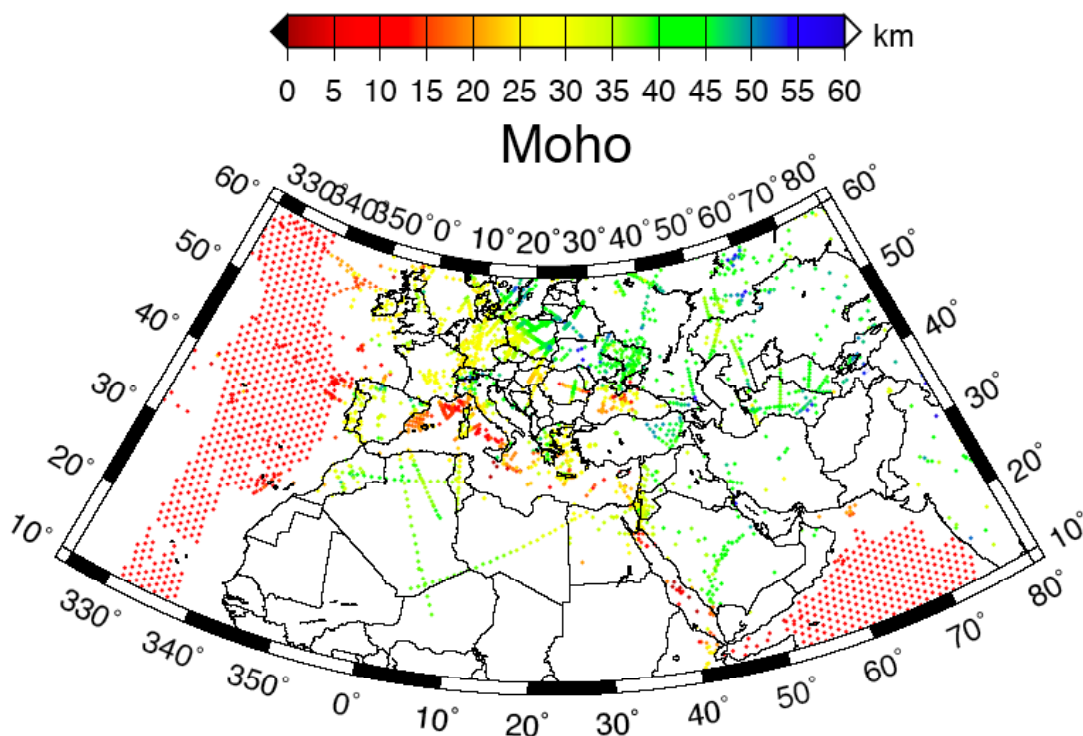
Crustal Thickness Constraints

Figure 4. Total point coverage for independent constraints on Moho depth used in our joint inversion. The points are color-coded with respect to a priori determined Moho depths.

While the fundamental-mode Rayleigh-wave group velocities and regional S and Rayleigh waveforms have significant sensitivity to Moho depth, they cannot uniquely resolve Moho depth. We therefore include independent estimates of crustal thickness as point constraints in the joint inversion and thus compile such measurements from a

large number of published studies. A partial list of these studies is provided in Marone et al. (2003), and part of these points stem from the database used for CRUST5.1. We have added new estimates of Moho depth from more recent studies and interactively resolved or removed conflicting data and outliers from the data set. The majority of this data set is from receiver function studies. Remaining points are from active-source studies and some are from gravity surveys. The active-source constraints were assigned the lowest error and the Moho-depth estimates from gravity were assigned the largest errors. For the oceans we use a constraint of 10 km for Moho depth, but only for points also covered by data from our other data sets.

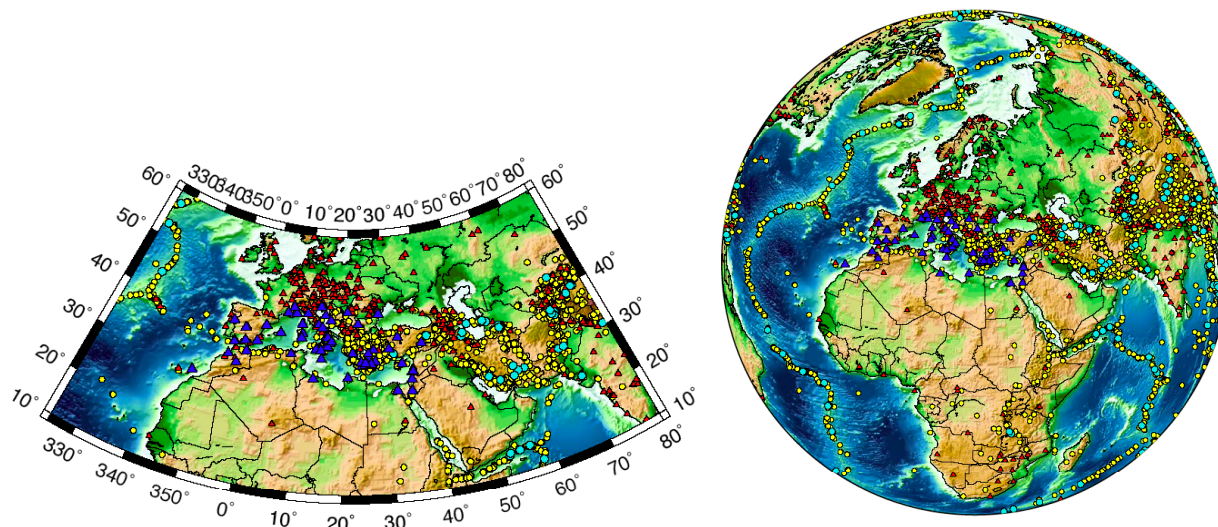## Teleseismic *S*-wave Arrival Times

Figure 5. Earthquakes (circles) and stations (triangles) for which we have teleseismic S-wave travel-times in our joint inversion. Blue stations and cyan events are used for cross-correlation measurements and red stations and yellow events are from Engdahl's (Engdahl et al., 1998) database of arrival picks.

Figure 5 shows a map of all stations and earthquakes that produced S-wave arrival times that we use in our joint inversion. The majority of these are from Engdahl's reprocessed ISC data set spanning 38 years of recording. Nevertheless, because of their heterogeneity, these arrival times were assigned a higher error than those we measured through cross-correlation. The waveforms of teleseismic S recorded at MIDSEA and other stations in the study region were cross-correlated with the method of VanDecar and Crosson (1990), yielding high-accuracy relative S-wave arrival times. Figure 6 shows those portions of the teleseismic S-wave paths in our data set that lie within a half degree from the cross section. Both cross sections show large data gaps in the upper mantle beneath Arabia and North Africa, illustrating the rationale for jointly inverting these data with surface wave data, which are sensitive to upper-mantle structure all along their way from event to station. The cross sections in Figure 6 show that the top of the lower mantle is well covered by these data and that the ray paths are near-vertical in the uppermost mantle, providing excellent lateral resolving power. This lateral resolving power excellently complements the vertical resolving power of the regional S and Rayleigh waveform fits. Resolving Moho depth from uppermost mantle and crust velocities is aided by the independent constraints on the Moho and the fundamental-mode group velocity measurements.
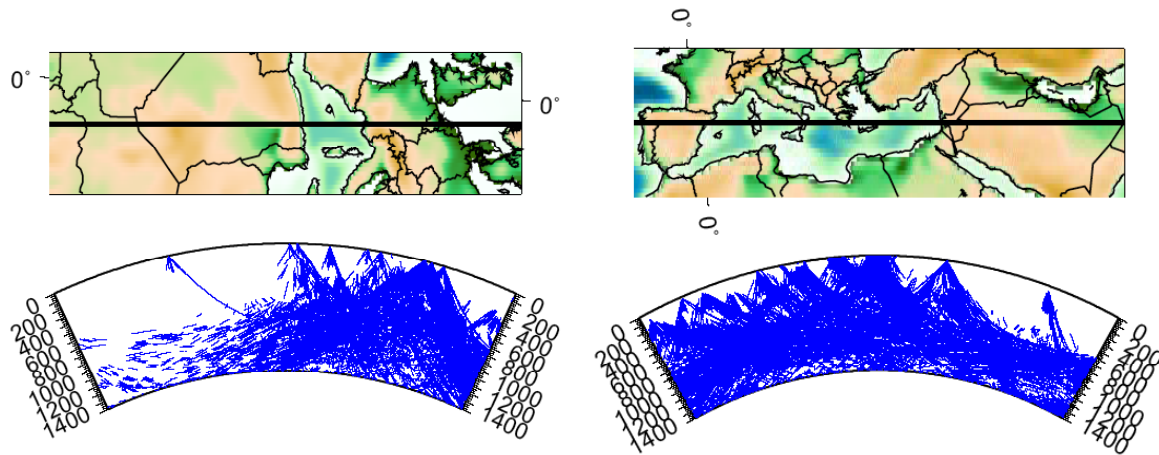
Figure 6. A NS and EW cross section through the study region showing segments of ray paths of teleseismic S waves used in our joint inversion that lie within half a degree from the cross section.
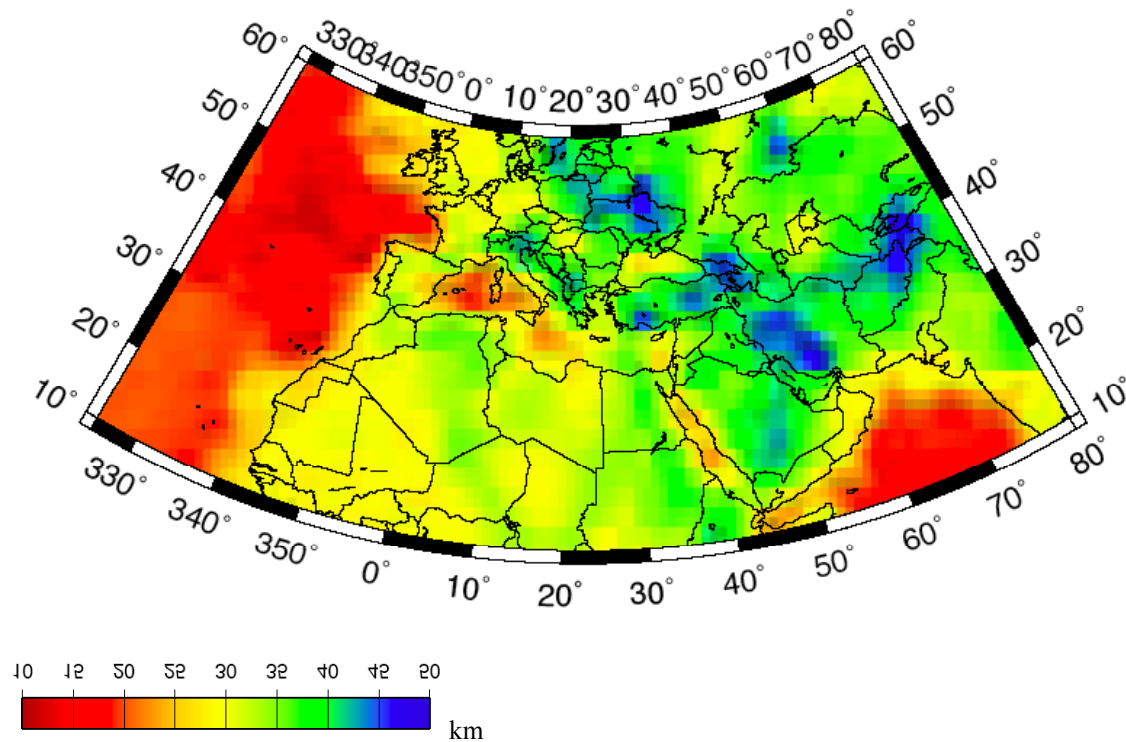
Inversion Results

Figure 7. Moho map from joint inversion of Moho constraints (Figure 4), regional waveform fits (Figure 2), Rayleigh wave group velocities (Figure 3), and teleseismic arrival times (Figure 5).

The benefit of our joint inversion lies in the fact that the different types of data sets we use cover the same general volume of the mantle and crust along the Tethys suture but cover the volume in very different, but complementary ways; our data sets are both redundant and complementary. The redundancy is needed to increase accuracy and to ensure that all data sets measure the same structural phenomena. The data sets need to be complementary to increase resolving power over a larger volume of mantle and crust and thereby reduce trade-offs inherent in each type of

seismic data set. Combining the data sets therefore not only enhances resolving power where the region is covered by more than one data sets, but resolution is also enhanced in the regions covered by only one data set (such as the lower mantle or the upper crust) because of the reduced trade-offs with other regions of the model.

We have developed software that handles the joint inversion of constraints from regional waveform fits, crustal estimates, group velocities, and teleseismic arrival times. An early version of the joint inversion code has been tested on the teleseismic *S* arrival time data set of Schmid et al. (2006) and the data derived from regional waveform fitting from Marone et al. (2004). The results show only a percent or two increase in the variance reduction obtained in the linear inversion of both data sets compared to their individual inversions (Schmid et al., 2006). The resolving power of the joint data sets, however, has increased dramatically: the teleseismic data add more lateral resolution to the regional waveform data, while the regional waveform data add more depth resolution to the teleseismic data. The resolved depth range of the combined data sets has doubled with respect to their individual depth ranges. The regional waveform data resolve the upper mantle more strongly while the teleseismic arrival times resolve the lower mantle more strongly. The resolving power of the combined data is superior to that of each of the data sets alone. The joint inversion reduces the variance in the data sets by 40 % for the teleseismic delay times, 50 % for the Rayleigh-wave group velocities, 75 % for the Moho point constraints, and 90 % for the regional waveform fits.

Figure 7 shows the joint inversion result for Moho depth. The map shows a good resemblance with the point constraints in Figure 4, but is much smoother because the regional waveforms and group velocity data, as well as regularization constraints in the joint inversion provide a smooth interpolation between the point constraints. The map is also broadly consistent with CRUST2.0, except in northern Africa, where the crust from our joint inversion is about 5 km thinner. Resolution tests indicate that our combined data sets can resolve the crustal thicknesses of CRUST2.0.
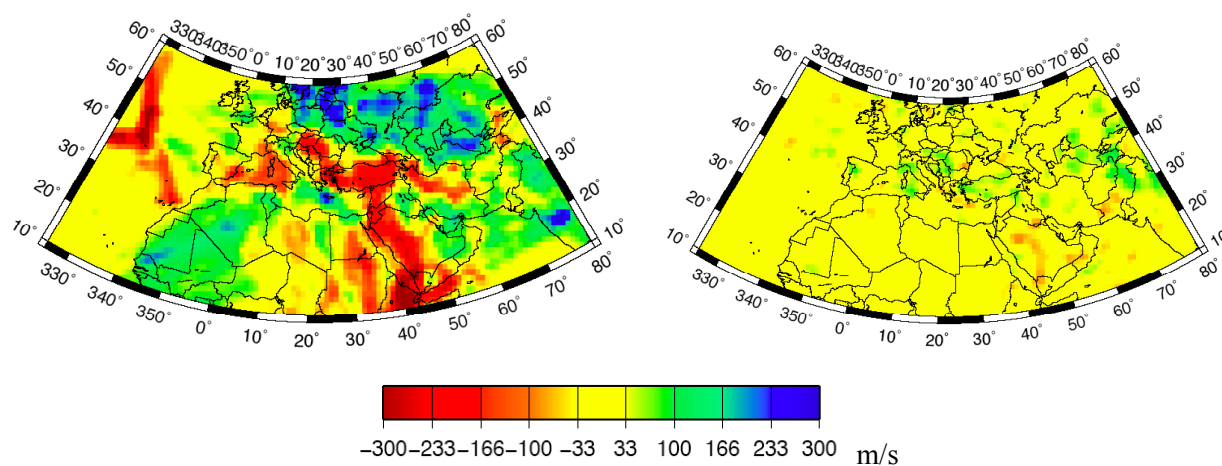

Figure 8. S-velocity perturbations relative to 1-D model MEAN (Marone et al., 2004) at a depth of 100 km (left) and 700 km (right) from our joint inversion.

The left panel of Figure 8 shows upper mantle shear velocity anomalies from the joint inversion at a depth of 100 km. The Mid-Atlantic Ridge, Algero-Provencal and Pannonian Basins, Tyrrhenian and Aegean Seas, Arabian and Nubian shields, and the Anatolian and Iranian Plateaus are underlain by significant low velocities. High velocities are imaged beneath the West-African Craton, to the northeast of the Tornquist-Tesseire Zone, beneath the Hellenic and Calabrian Arcs, and beneath the Arabian Platform and Zagros Fold Belt. The right panel of Figure 8 shows that the anomalies get weaker below the upper mantle and are dominated by high-velocity anomalies in the top of the lower mantle. These high-velocity anomalies appear to form an EW belt, roughly parallel to the Tethys suture.

CONCLUSIONS AND RECOMMENDATIONS

The broad consistency between seismic velocity anomalies inferred from teleseismic arrival times, Rayleigh wave group velocities, and regional waveforms shown here implies that these different types of data sets have recorded the same structural phenomena, despite differences in size and character between typical sensitivity kernels for each data set. This conclusion is further supported by an analysis of how teleseismic delay times depend on frequency (Schmid et al., 2006) and that the teleseismic arrival times and the regional waveforms are highly complementary. The shared sensitivity, though different in character, of receiver functions and Rayleigh wave group velocities to crustal structure helps to separate crustal effects on the observed data from mantle effects, when included in the joint inversion.

Through a joint inversion of teleseismic S-wave arrival time delays, waveform fits of regional S- and Rayleigh waves, group velocity measurements of fundamental-mode Rayleigh waves, and independent constraints on Moho depth, we have achieved considerable variance reduction in each data set simultaneously. The 3-D S-velocity model resulting from this joint inversion shows high and low-velocity anomalies that are broadly consistent with previous studies, restricted to a smaller region or a more limited data set. Our new model may be converted to a P-velocity model and used for locating events.

Our final steps in this project are to carry out this conversion to P-velocities and computing arrival time surfaces and synthetic seismograms for the purpose of potentially improving event location procedures.

ACKNOWLEDGEMENTS

REFERENCES

Bijwaard, H., W. Spakman, and E.R. Engdahl (1998), Closing the gap between regional and global travel time tomography, *J. Geophys. Res.* 103: 30055–30078.

DeMets, C. R.G. Gordon, D.F. Argus, and S. Stein (1990). Current plate motions, *Geophys. J. Int*. 101: 425–478.

Engdahl, E.R., van der Hilst, R. and Buland, R. (1998). Global teleseismic earthquake relocation with improved travel times and procedures for depth determination, *Bull. Seis. Soc. Am*. 88: 722–743.

Julia, J., C. Ammon and R. Herrmann (2003). Lithospheric structure of the Arabian Shield from the joint inversion of receiver functions and surface wave group velocities, *Tectonophysics* 371: 1–21.

Maggi, A. and K. Priestley (2005). Surface waveform tomography of the Turkish-Iranian Plateau, *Geophys. J. Int*. 160: 1068–1080.

Marone, F. S. van der Lee, and D. Giardini (2003). Joint inversion of local, regional, and teleseismic data for crustal thickness in the Eurasia-Africa plate boundary region, *Geophys. J. Int*. 154: 499–514.

Marone, F., S. Van der Lee, and D. Giardini (2004). 3-D upper mantle *S*-velocity model for the Eurasia-Africa plate boundary region, *Geophys. J. Int*. 158: 109–130.

Mokhtar, T. and M. Al-Saeed (1994). Shear wave velocity structures of the Arabian Peninsula, *Tectonophysics* 230: 105–125.

Mooney, W.D., G. Laske, and T.G. Masters (1998). CRUST 5.1: A global crustal model at 5° x 5°, *J. Geophys. Res*. 103: 727–747.

Nolet, G. (1990). Partitioned waveform inversion and 2-dimensional structure under the network of autonomously recording seismographs, *J. Geophys. Res*. 95: 8499–8512.

Pasyanos, M. E. (2005). A varible-resolution surface wave dispersion study of Eurasia, North Africa, and surrounding regions, *J. Geophys. Res*. 110: B12301, doi:10.1029/2005JB003749.

Rodgers, A., W. Walter, R. Mellors, A. M. S. Al-Amri and Y. S. Zhang (1999). Lithospheric structure of the Arabian Shield and Platform from complete regional waveform modeling and surface wave group velocities, *Geophys. J. Int.* 138: 871–878.

Schmid, C., S. van der Lee, and D. Giardini (2006). Correlated shear and bulk moduli to 1400 km beneath the Mediterranean region, *Phys. Earth Planet. Sci. Lett.* 159: 213–224.

Schmid, C., S. van der Lee, J. C. Vandecar, E. R. Engdahl, and D. Giardini (2007). 3-dimensional S-velocity of the mantle in the African-Eurasia plate boundary region from phase arrival times and regional waveforms, *J. Geophys. Res*., in press.

Sandvol, E., D. Seber, M. Barazangi, F. Vernon, R. Mellors, and A. Al-Amri (1998). Lithospheric seismic velocity discontinuities beneath the Arabian Shield, *Geophys. Res. Lett*. 25: 2873–2876.

VanDecar, J.C., and R.S. Crosson (1990). Determination of teleseismic relative phase arrival times using multi-channel cross-correlation and least-squares, *Bull. Seism. Soc. Am*. 80: 150–169.

Van der Lee, S. (1990), Tomographic inversion of delay times for P-velocities beneath Europe, *Master's thesis*, Utrecht University, 97 pp.

Van der Lee, S. and G. Nolet (1997). Upper-mantle S-velocity structure of North America, *J. Geophys. Res*. 102: 22,815–22,838.

Van der Lee, S., F. Marone, M. van der Meijde, D. Giardini, A. Deschamps, L. Margheriti, P. Burkett, S. C. Soloman, P. M. Alves, M. Chouliaras, A. Eshwehdi, A. Suleiman, H. Gashut, M. Herak, R. Oritz, J. M. Davila, A. Ugalde, J. Vila, and K. Yelles (2001), Eurasia-Africa plate boundary region yields new seismographic data, Eos Trans. AGU, 82: (51), 637–646.